The influence of soil nonlinear properties on the track/ground vibration induced by trains running on soft ground

J. Y. Shih[1,*], D.J. Thompson[1], A. Zervos[2]

1: Institute of Sound and Vibration Research, Faculty of Engineering and the Environment, University of Southampton, Southampton, SO17 1BJ, UK.

2: Infrastructure Research Group, Faculty of Engineering and the Environment, University of Southampton, Southampton, SO17 1BJ, UK.

*: corresponding author; email: j.shih@hud.ac.uk
Now at: Institute of Railway Engineering Research, Faculty of Computing and Engineering, University of Huddersfield, Huddersfield, HD1 3DH, UK

Abstract

The deflections of the track under a moving train depend on the stiffness of the underlying soil as well as the properties of the track and the train. In many situations, small-strain linear properties can be assumed for the soil. However, particularly for soft soil, as the load speed approaches the speed of Rayleigh waves in the ground, the deflections increase considerably. In such situations the use of the small-strain soil stiffness may lead to inaccuracies in the estimates of track deflections or of the critical speed. A finite element model of the track and ground has been developed to study the deflections induced by trains running on soft ground. Soil nonlinearity is introduced through a user-defined subroutine. The nonlinearity is specified in terms of the shear modulus reduction as a function of octahedral shear strain, which can be based on data obtained from laboratory tests on soil samples. The model is applied to the soft soil site at Ledsgård in Sweden, from which extensive measurements are available from the late 1990s. It is shown that the use of a linear model based on the small-strain soil parameters leads to an underestimation of the track displacements when the train speed approaches the critical speed, whereas the nonlinear model gives improved agreement with measurements. In addition, an equivalent linear model is considered, in which the equivalent soil modulus is derived from the laboratory curve of shear modulus reduction using an 'effective' shear strain. For this approach it is shown that the predictions in this

specific case are improved by using a value of 20% of the maximum strain as the effective strain rather than the value of 65% commonly used in earthquake studies.

Key words: critical speed, equivalent linear model, effective shear strain, soil nonlinearity, soft soil

1. Introduction

High-speed railways have become an important means of public transport in many countries due to the demands of increasing population as well as environmental concerns. One potential problem with high-speed rail is that large displacements of the track occur when the train speed approaches the speed of waves in the ground and embankment, known as the critical speed [1]. Where the ground is especially soft, the critical speed may be as low as 50 m/s and the track displacements can be very large. These large displacements can lead to damage of the track components as well as a danger of derailment. As a result, accurate assessment of this effect is an important aspect of good high-speed railway design. In addition, better understanding of the stresses and strains in the subgrade and the amplitudes of vibration of the whole system can lead to reduced cost of maintenance and improved quality of the railway system.

A number of theoretical models have been developed by various authors in an attempt to understand and predict such phenomena. Approaches adopted include semi-analytical models [1]–[4] and numerical models [5]–[15] based on finite element (FE) and boundary element (BE) approaches. Both frequency domain [1]–[11] and time domain [12]–[15] approaches have been considered. Consideration of train/track dynamic interaction can usually be neglected for the low frequency displacements close to the track. However, consideration of vehicle/track interaction is important for ground-borne vibration in the far field and at higher frequencies [9]–[11].

In predicting environmental ground vibration from trains, linear elastic models of the soil are normally used, which is generally justified by the fact that the strains are small. However, as the train speed approaches the critical speed, the track deflections increase and nonlinear effects may become important especially in the vicinity of the track [1], [4], [5]. Of particular interest in this regard is the soft soil site at Ledsgård, south of Gothenburg in Sweden, where

field tests were carried out in the late 1990s with trains running at or near the critical speed [1], [4]. Extensive soil investigations were also carried out [5], [12].

From laboratory tests, soil stiffness is found to depend strongly on cyclic strain amplitude, as well as a number of other factors such as mean principal effective stress, plasticity index, void ratio, over-consolidation ratio, and the number of loading cycles [16]. In modelling nonlinear soil behaviour, it is particularly important to determine the dependence of the shear modulus on the strain, especially for shear strains larger than 10^{-5} to 10^{-4} [17]. Reductions in soil stiffness with increased strain level (known as stiffness degradation), and corresponding increases in damping ratio, can be determined using cyclic triaxial tests [16], [18]–[20]. These results can be described by a shear modulus reduction curve and a corresponding curve of damping ratio as a function of shear strain.

To include these effects in a model of the track and ground, several authors have used equivalent linear models [1], [4], [5], [12], [21]. These involve an iterative procedure that can approximate nonlinear behaviour efficiently. From an initial calculation, an 'effective' shear strain amplitude is determined from the time-varying strains. This is then used with the measured curves of shear modulus and damping at different shear strains to calculate updated values of the shear modulus and damping ratio corresponding to the motion. The model is run again until the strains obtained correspond to the assumed modulus. In order to characterise the motion, the value used for the effective shear strain in this process is chosen as a certain proportion of the maximum strain. It is important to determine this factor appropriately if the correct results are to be obtained from the equivalent linear model [22], [23]. Different values for this factor has been found empirically; for example 0.65 is usually recommended for seismic analysis [16]. However, overestimation of the amplitude, sometimes by more than 50%, has been found when using the value of 0.65 in situations where particularly large strains occur [22]. Depending on the situation, values between 0.2 and 1 have been found to give the best results [22], [24]. As the dynamic characteristics of the vibration induced by high-speed trains differ from those of earthquakes, further investigation is required.

In [1], [4], [12] such equivalent linear models were used for the soft soil site of Ledsgård. In these models the stiffness reduction, based on an approximate effective strain level, was applied to all elements within a given soil layer. A more advanced approach was implemented by Costa et al. [5] in which the shear modulus was adjusted according to the maximum effective shear strain in each element of the 2D cross-section, resulting in a

transverse inhomogeneity in the ground. It was found that a number of iterations were required to reach a value of shear modulus that was consistent with the corresponding strain level.

The nonlinear stress-strain behaviour of soils can be represented more accurately by cyclic nonlinear constitutive models that follow the actual stress-strain path during cyclic loading. This behaviour can be characterized by a backbone curve and a series of rules that govern the unloading-reloading behaviour, stiffness degradation, and other effects such as irregular loading, densification, pore pressure generation, etc. An early implementation of a nonlinear model for railway dynamics was that introduced by Sadeghi [25]. A nonlinear stress-strain model was developed including consideration of permanent strain and failure criteria using an extended Drucker-Prager plasticity model. The rail displacements from a nonlinear model were found to be 20% greater than those from a linear model due to the plastic strain in the substructure layer. However, this was a two-dimensional model which did not consider the moving load effect. A popular cyclic model for soil was given by Iwan [26]. This used a series of parallel Jenkin elements, which consist of a linear spring in series with a frictional slider, to describe the backbone curve and the yield level. This model was adopted by Gomes Correia and Cunha [27] to study the effect of subgrade nonlinearity on the track response induced by a high-speed train. Such cyclic models can also represent the development of permanent strains, hardening under drained conditions or stiffness degradation under undrained conditions due to pore pressure development. A more complex nonlinear model was used by Fernandes [28] to represent the ballast and soil beneath a railway track. The dynamic response was obtained after five cycles of loading due to moving axles and permanent displacements were determined for understanding the behaviour of the soil and ballast degradation. Another advanced model was adopted by Kalliainen et al. [29] based on the nonlinear material constitutive model based on the strength parameters developed by Indraratna et al. [30] for the ballast, embankment and ground. An investigation of fresh and poor ballast and different ground properties was presented. Recently, Woodward et al. [31] considered a non-linear model for the resilient modulus based on the mean and shear stresses and a nonlinear damping ratio based on the deviatoric strain to investigate the influence of considering nonlinearity when assessing critical speed effects for soft ground. Despite these various developments, all these models are very complex and require many parameters to construct the soil constitutive model.

A simpler nonlinear model is introduced here that is based on the shear modulus reduction curve that can be obtained from laboratory tests. At each time step the soil stiffness in each element is determined based on the instantaneous octahedral shear strain. This is implemented in a user-defined subroutine within the FE software ABAQUS. Plastic behaviour is not considered here as it can be considered to be small compared with the transient dynamic deflections and the objective is not to study long-term track settlement. Finally, the results are compared with site measurements from Ledsgård [5]. The influence of the soil nonlinearity on the critical speed and stress-strain behaviour of the embankment and ground is investigated. Furthermore, the use of equivalent linear analysis for the moving train problem is discussed and the appropriate factor for determining the effective shear strain is investigated.

2. Nonlinear model

During cyclic loading, the stress-strain behaviour of the soil typically follows a nonlinear hysteresis loop, as shown schematically in Fig. 1. The slope of the stress-strain curve can be identified as the soil stiffness or modulus. The dissipated energy, which is related to the damping ratio, can be determined from the area of the loop. The secant shear modulus G_{sec} is defined from the maximum values of stress and strain as indicated in Fig. 1. As the amplitude of the loading increases, it can be seen that this modulus reduces in the example shown, with the maximum shear modulus G_{max} occurring for very small amplitudes. The ratio of the secant shear modulus at a given strain level to the maximum shear modulus can be identified as the shear modulus reduction. Fig. 2(a) shows shear modulus reduction curves obtained from cyclic triaxial tests at different amplitudes, for material samples obtained at Ledsgård [5]. In contrast to the stiffness, the damping ratio tends to increase when the strain level increases, as shown in Fig. 2(b).
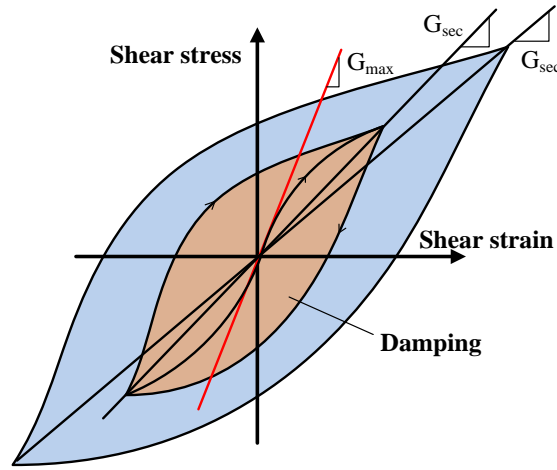
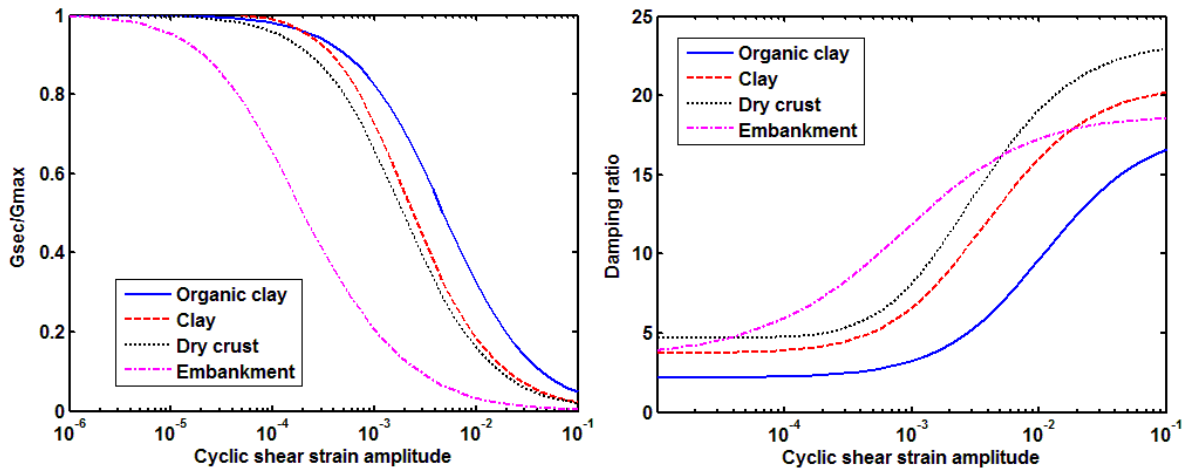Figure 1. Shear-strain path during cyclic loading

Figure 2. Nonlinear soil characteristics obtained for different soil layers at Ledsgård [5] (a) shear modulus reduction curves; (b) damping ratio

Shear modulus reduction curves such as these have been defined by fitting empirical formulae [18] to experimental data. These functions have then been implemented through a user-defined material subroutine UMAT in the commercial finite element program, ABAQUS, to give a nonlinear constitutive material model. For each integration point within a finite element, the subroutine receives variables such as the incremental strain vector and the previous stress vector, and returns the current stress vector and updated Jacobian matrix (i.e. the current tangent modulus matrix). The new shear modulus is obtained from the modulus reduction curve, which is expressed in terms of the shear strain value. However, due to the fact that in general the deflection involves multiple strain components, the octahedral shear strain is used as the strain index to evaluate the value of modulus reduction for each time step. This is given by

$$\gamma_{oct} = \frac{1}{3}\sqrt{\left(\varepsilon_{xx} - \varepsilon_{yy}\right)^2 + \left(\varepsilon_{yy} - \varepsilon_{zz}\right)^2 + \left(\varepsilon_{xx} - \varepsilon_{zz}\right)^2 + 6\left(\gamma_{xy}^2 + \gamma_{yz}^2 + \gamma_{xz}^2\right)} \qquad (1)$$

where ε_{xx}, ε_{yy} and ε_{zz} are the strains in the three coordinate directions and γ_{xy}, γ_{yz} and γ_{zx} are the shear strains. From the new shear modulus, determined from the modulus reduction curve, the new constitutive matrix is obtained and hence the stress vector can be updated at the next time step $i+1$ using

$$\{\sigma\}_{i+1} = [D]_i \{\varepsilon\}_i \qquad (2)$$

where $\{\varepsilon\}_i$ is the strain vector and $[D]_i$ is the constitutive matrix at time step i.

To include damping in the nonlinear model, Rayleigh damping is used in which the damping matrix is proportional to the mass and stiffness matrices, $[M]$ and $[K]$, with the factors α and β as follows

$$[C] = \alpha[M] + \beta[K] \qquad (3)$$

The values of α and β are chosen to match the damping ratio to a certain value ξ at two representative frequencies, ω_1 and ω_2, giving

$$\alpha = \frac{2\xi\omega_1\omega_2}{\omega_1 + \omega_2}, \qquad \beta = \frac{2\xi}{\omega_1 + \omega_2} \qquad (4)$$

For a constant value of α, the mass-proportional component of damping can be incorporated directly using the ABAQUS FE code for built-in constitutive models. However, for a user-defined material, the stiffness-proportional damping must be incorporated within the user-defined material subroutine. This can be achieved by adding the corresponding stress term:

$$\{\sigma_d\}_{i+1} = \beta[D]_i \{\dot{\varepsilon}\}_i \qquad (5)$$

where $\dot{\varepsilon}$ is the strain rate. This term is added to the stress resulting from the elastic responses at each integration point. As a result, the total stress is given by adding Eq. (2) and (5).

In the present work only constant values of α and β are used. For a constant value of β, the stiffness-proportional term will reduce as the stiffness degrades. However, for a constant value of α, the mass-proportional term corresponds to an increasing value of damping ratio as

the stiffness degrades. This can be seen for a single degree of freedom system with natural frequency ω_0, mass m and stiffness k_i at time step i; the damping ratio is given by

$$\xi_i = \frac{\alpha m \omega_0}{2k_i}$$

(6)

Consequently, when the stiffness degrades, it is found that the damping ratio will increase. Although β has a greater influence at higher frequencies, α dominates the damping ratio for the lower frequencies which are more relevant in the present calculations. As a result, the damping ratio in the model will increase according to the inverse of the shear modulus reduction.

3. Numerical model

A three-dimensional FE model has been constructed of the track and ground at the site at Ledsgård. Soil properties are available from various in-situ tests, including cross-hole tests, Spectral Analysis of Surface Waves (SASW) and Seismic Cone Penetration Testing (SCPT) [5], [12]. In addition to the embankment, three main soil layers were identified, referred to as dry crust, organic clay, and clay. Measured shear wave speeds as a function of depth are shown in Fig. 3(a) along with the values assumed here. The cross-section of the model is shown in Fig. 3(b). The lower clay layer is assigned a shear wave speed that varies with depth. The material properties used for the various layers are listed in Table 1.

The FE mesh used is shown in Fig. 4. Use is made of symmetry about the track centreline. A cuboid model is used, with fixed boundaries, a width of 40.5 m and a depth of 33.2 m, see Fig. 3(b). The length of the model required to achieve convergence to steady state depends on the load speed [32], with longer models required if the load speed approaches or exceeds the critical speed. Here, the model is 80 m long, which is found to be sufficient for convergence. It has been found previously that, provided that the model is wide enough, there is little benefit in using absorbing elements at the boundaries [32], [33]. This relies on using a damping model with a sufficiently large mass-proportional term, allowing the energy to be dissipated sufficiently to avoid the reflections interfering with the results [32]. The target low-strain damping ratios for the four different materials are listed in Table 1 based on dynamic triaxial and cross-hole tests [5], [12]. The nonlinear model includes the shear modulus reduction curves shown in Fig. 2.
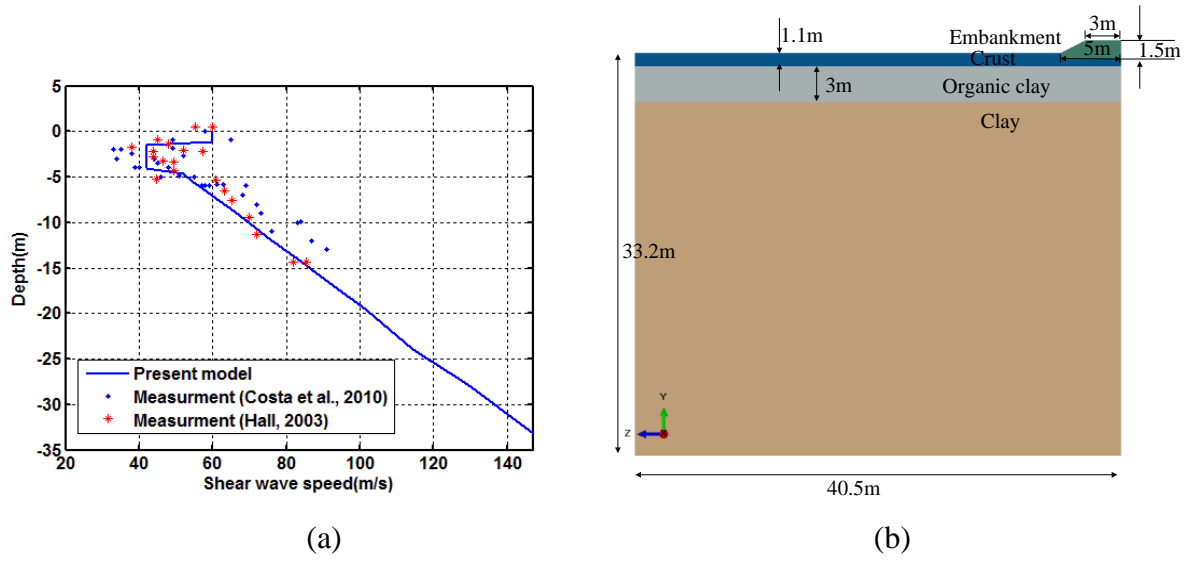
Figure 3. Soil and railway embankment geometry and shear wave speed at Ledsgård based on soil investigations[5], [12]; (a) shear wave speed; (b) cross-section
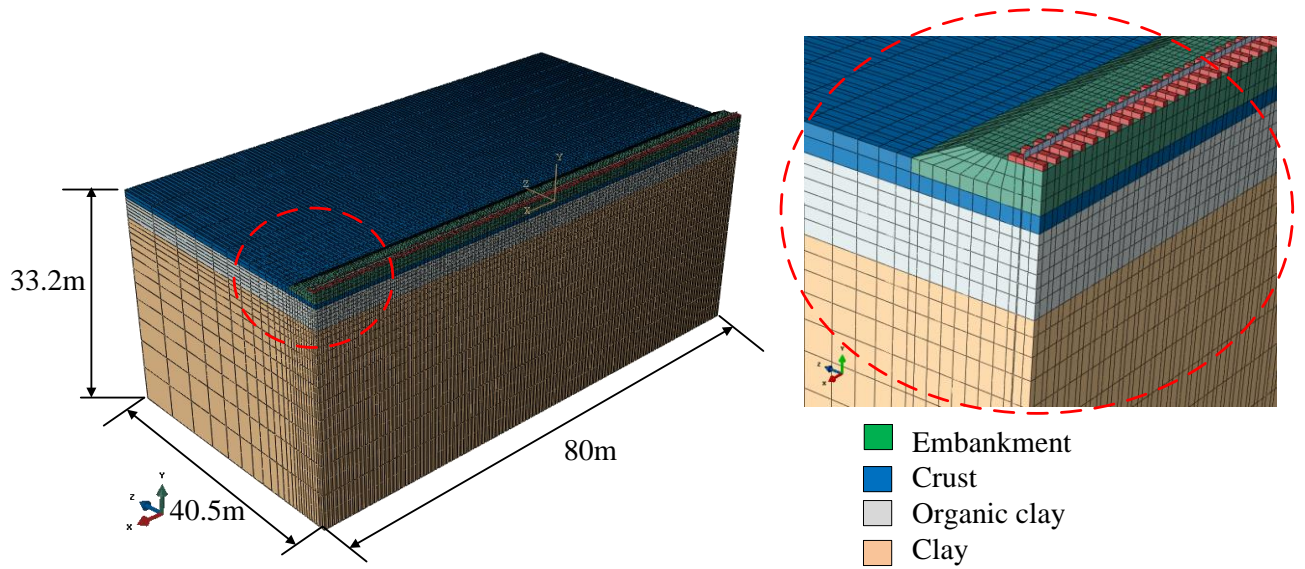

Figure 4. Three-dimensional track/ground model

The chosen Rayleigh damping coefficients are shown in Table 2; these are obtained from Eq. (4) using target frequencies of 3 and 20 Hz. This gives damping ratios close to the target values between these frequencies. This frequency range is chosen to correspond to region where the measured vibration spectra close to the track has its maximum [5], [12].

Fully-integrated quadratic cuboid finite elements are used for the whole ground model, while linear Timoshenko beam elements are used for the UIC60 rail. To represent the railpads, linear springs with vertical stiffness 4.7×10^8 N/m are used to connect the rail to each sleeper. Discrete sleepers with a spacing of 0.67 m are included. The sleepers have a half-length of

9

1.3 m, a height of 0.2 m, mass density 2500 kg/m^3, Young's modulus 3×10^{10} N/m^2 and Poisson's ratio 0.15. The ballast is included as part of the embankment layer and this in turn is embedded to a depth of 0.4 m into the upper ground layer. The smallest element size is set to be 0.5 m in the vicinity of the track, which is sufficient for accurate modelling of local deflections up to at least 20 Hz. However, the element size is gradually increased with a stretch factor of 1.2 in the horizontal direction outside the width of the track, and in the vertical direction for the clay layer, as shown in Fig. 4. This prevents the model from becoming too large and has been found to be acceptable provided that far-field wave propagation is not of interest. The total number of degrees of freedom in the model is 1.76 million.

Table 1. Embankment and ground properties

	Thickness	P-wave speed	S-wave speed	Shear modulus	Density	Damping ratio
Embankment	1.5 m	470 m/s	250 m/s	112.5 MPa	1800 kg/m^3	12%
Crust	1.1 m*	500 m/s	60 m/s	5.4 MPa	1500 kg/m^3	7%
Organic clay	3.0 m	500 m/s	42 m/s	2.2 MPa	1250 kg/m^3	4%
Clay	29.1 m	1500 m/s	50~122.9 m/s	3.7~22 MPa	1470 kg/m^3	7%

*: 0.5 m under embankment

Table 2. Embankment and ground Rayleigh damping coefficients

	α	β
Embankment	4.5	0.0015
Crust	2.64	0.001
Organic clay	1.553	0.0006
Clay	2.64	0.001

Results are presented for a set of moving axle loads; surface roughness excitation is neglected. Details of the train, X2000, are available from the literature [5]; a summary is given in Table 3. Multiple loads are applied on the rail at the locations of the various axles and these are moved along the track according to the train speed. The axle load is applied continuously along the rail. In the experiments [5] the train ran in both directions. To represent the northbound train, with the locomotive leading, only two vehicles (eight axles) are considered, because the maximum deflections occurred for the front vehicle. However, the full train set consisting of a driving trailer vehicle, three passenger carriages and a locomotive is considered for analysis of the southbound direction. For linear analysis it is sufficient to

model a single moving load and to use superposition to determine the response to the whole train but for nonlinear analysis this is no longer possible.

Table 3. Details of X2000 high speed train used in field tests [5]

	Length		Axle load
Locomotive	16.5 m	1st bogie axle loads	181 kN
		2nd bogie axle loads	180 kN
3 × passenger carriages	24.7 m	3rd ~ 8th bogie axle loads	122 kN
Driving trailer	21.5 m	9th bogie axle loads	117 kN
		10th bogie axle loads	160 kN

4. Results for nonlinear models

In this section results are presented from two nonlinear models as well as a linear model based on the unreduced parameters given in Table 1. These results are compared with measurements from Ledsgård [5].

4.1 Parameters for nonlinear models

The parameters for the organic clay are the most important for the behaviour of the whole system, as this is the softest layer, see Table 1. Measurement data for this material, obtained from triaxial tests [5], is shown in Fig. 5 in the form of the shear modulus reduction and damping ratio. Significant scatter can be observed in these experimental results. Two lines are given, based on an empirical equation proposed by Ishibashi et al. [18] (see Appendix A). These are fitted approximately to the data by choosing appropriate values of mean effective confining pressure and plasticity index. The mean effective confining pressure is set to 300 kPa and the plasticity index is set to 100 for nonlinear model 1 and 140 for nonlinear model 2. These functions are used in the material constitutive model described in Section 2 to represent the soil nonlinearity. The same constant value is used for Rayleigh damping (see Table 2) for both nonlinear models. As discussed in Section 2, the resulting damping ratio will increase according to the inverse of the shear modulus reduction based on Eq. (6), as shown in Fig. 5(b). It can be observed that the second nonlinear model fits the damping ratio data better than the first, although both give a reasonable fit to the modulus reduction data.
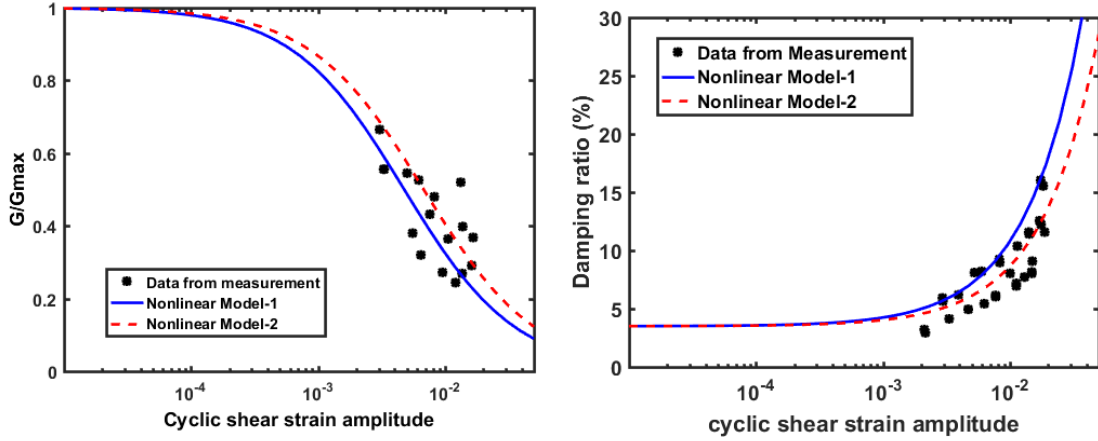
Figure 5. Shear modulus reduction curve and damping ratio for organic clay layer; (a) shear modulus reduction; (b) damping ratio

4.2 Track displacements from nonlinear models

The results from these two nonlinear models, as well as the linear model, are compared with the measurements in Fig. 6 for a train speed of 50 m/s. As discussed above, for the northbound direction only the two leading vehicles are considered in the model. Good agreement with the measurements is found by using the second nonlinear model, which is somewhat stiffer than the first one. The peak deflection from the first nonlinear model is almost double that from the second one. On the other hand, the results from the linear model tend to be too small compared with the measurement.
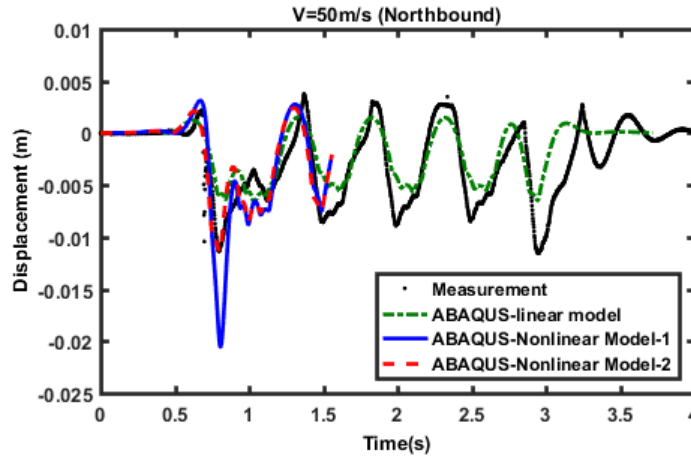

Figure 6. Displacement for northbound train: comparison between linear, nonlinear models and measurement for load speed 50 m/s

Fig. 7 shows the results from the two nonlinear models for the northbound direction for three different load speeds, 19 m/s, 45 m/s and 50 m/s. As can be seen, at the lower speed the two nonlinear models give very similar results. On the other hand, significant differences can be
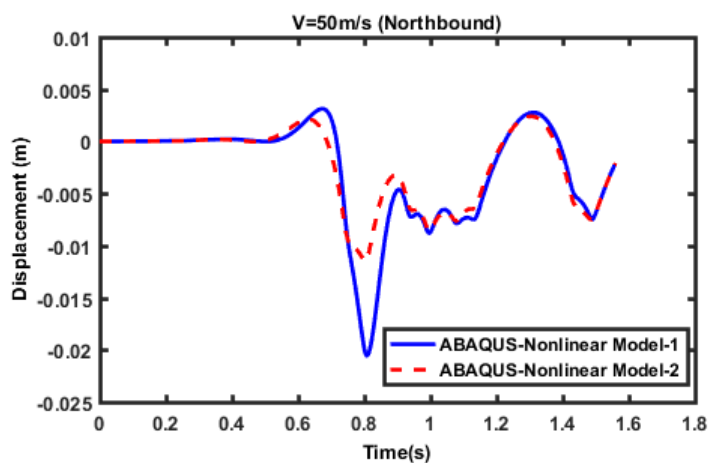
found between them for the load speeds of 45 m/s and 50 m/s at the position of the first bogie, whereas the differences are much smaller at other positions.
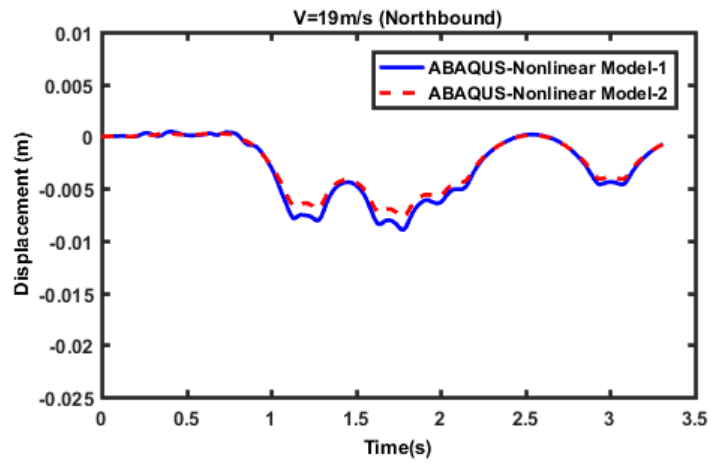

(a)
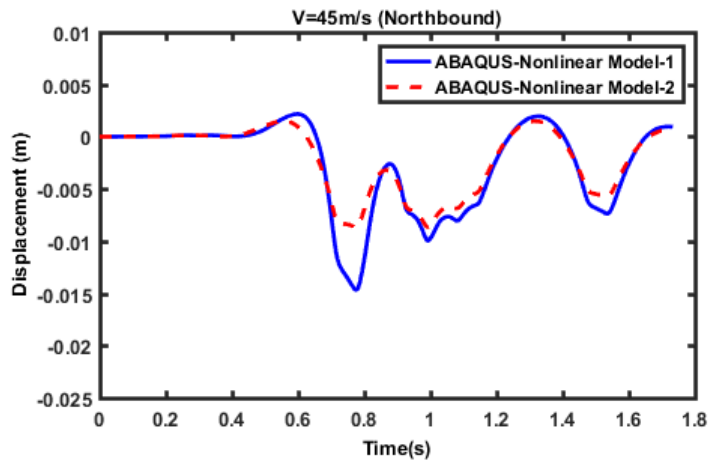
(b)

(c)

Figure 7. Northbound displacement comparison between two nonlinear models for different load speeds; (a) V=19 m/s; (b) V=45 m/s; (c) V=50 m/s

The results from the lower speed (see Fig. 7(a)) correspond approximately to the results obtained from a static analysis. The deflection under each axle can be discerned, with a nearly symmetric pattern of deflection under each bogie. Although the first four axles, which are on the locomotive, have equally high loads, the maximum deflection occurs at the position of the fourth axle due to the influence of the adjacent axles in the second and third bogies. On the other hand, at higher speeds (see Fig. 7(b)~(c)) the maximum deflection occurs at the leading axle and the deflection pattern becomes non-symmetric.

When the first load is suddenly applied, large strains occur in the surface layers immediately beneath the load, leading to stiffness degradation and particularly high track deflections for the softer nonlinear model 1. The region of influence is limited by the low wave speed in the soil. Subsequently, this deflection spreads into adjacent areas of the soil so that the region of influence increases and the local strains are lower for the later axle loads, leading to smaller stiffness degradation.

Fig. 8 shows the results for the southbound direction for two different load speeds. Here the full train is simulated. Fig. 8(a) compares the track deflections under the train with measurements for 19 m/s, showing good agreement even for the linear model. The results from the nonlinear models (not shown) are similar. In contrast, as shown in Fig. 8(b), for a train speed of 56.7 m/s the results from the linear model are around 40% smaller than the measurements, whereas the second nonlinear model gives good agreement.
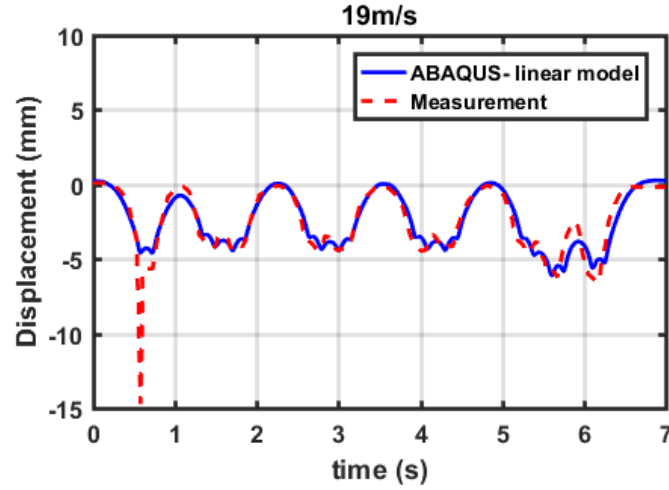
(a)
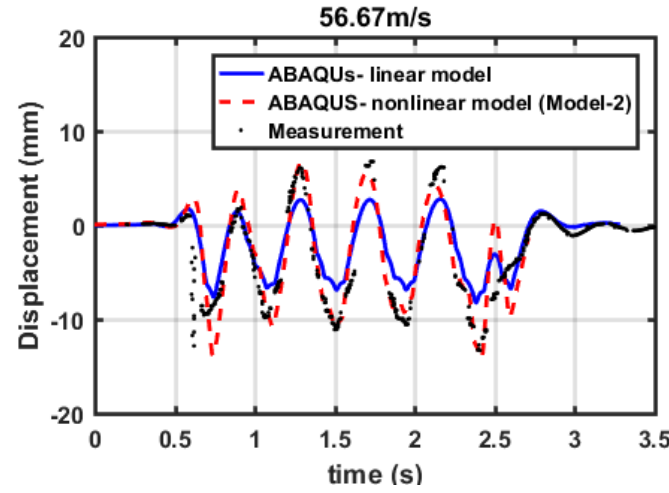
(b)

Figure 8. Southbound displacement from linear model for two different speeds; (a) V=19m/s; (b) V=56.7m/s

4.3 Assessment of octahedral shear strain

At high speed, the maximum strain level occurs at the position of the first axle load of the locomotive; for the first nonlinear model in Fig. 6 it is around double that found from the second nonlinear model. This can also be seen in Fig. 9, which shows the octahedral shear strain on the top surface of the organic clay layer for the two different nonlinear models. The results are in the spatial domain at a specific time step (when the results have achieved steady state) so the x coordinates are arbitrary. The strain distribution behind the region of maximum strain is very similar in the results from the two nonlinear models, with strain values around 0.18% from the first nonlinear model and 0.15% from the second one. This is due to the fact that the differences between the two shear modulus reduction curves are smaller for lower strain levels, as shown in Fig 5. For example, for a strain level of 0.1% the modulus reduction

15

is 0.83 for the first nonlinear model and 0.88 for the second nonlinear model. However, when strain level increases to 0.5%, the modulus reduction for the first nonlinear model drops to 0.48 but it is 0.6 for the second one. As a result, larger differences can be found when the strain level exceeds 0.1%.
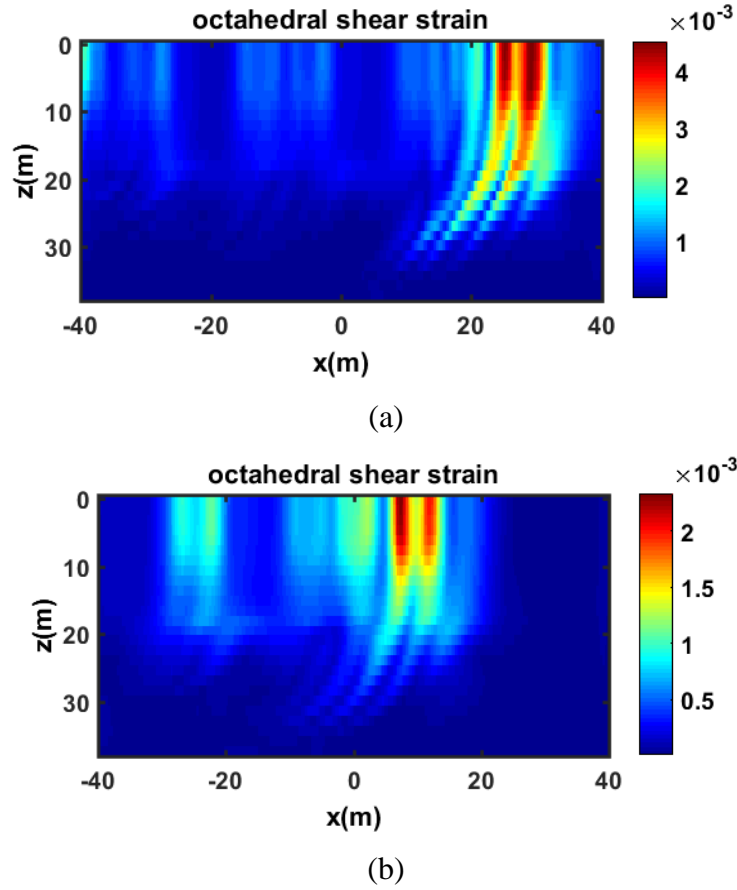

(a)

(b)

Figure 9. Octahedral shear strain on the top surface of organic clay layer when train speed is 50 m/s for two different nonlinear models (northbound); (a) nonlinear model 1; nonlinear model 2

The responses below the rail at the top of the organic clay layer are shown in Fig 10. This shows more clearly the difference between the two nonlinear models. Here, the *x*-coordinate of the results from nonlinear model 2 have been aligned with those from nonlinear model 1. The strain increases further when the soil becomes softer. Consequently, the maximum strain level from the first nonlinear model is around double that from the second one, as also found for the displacement in Fig. 6. In the remainder of the results only nonlinear model 2 is considered.
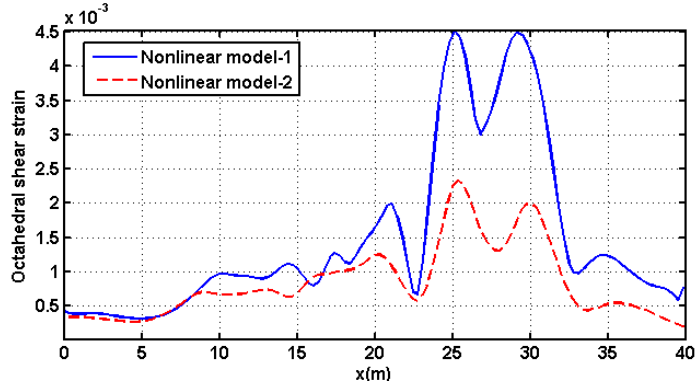
Figures 10. Octahedral shear strain variation below the rail on the top surface of the organic clay layer from two different nonlinear models

To compare the results from linear and nonlinear models, the octahedral shear strain at the top surface of the organic clay layer is shown in Fig. 11 for a load speed at 56.7 m/s. The strain level from the nonlinear model is not only larger than that from the linear model but the shape of the deflection is different. A clear wave-shaped pattern occurs for the nonlinear model. This is because the load speed is higher than the wave speed in the ground in this case, whereas for the linear model it is still below the critical speed (see Section 4.2 below). It is clear that this effect is larger for the nonlinear model at 56.7 m/s than at a speed of 50 m/s in Fig. 9(b). Furthermore, even though the strain levels decrease further away from the track, octahedral shear strains of around 10^{-3} can still be found at 30 m away from the track for the nonlinear model, as shown in Fig. 11(b), while even for the linear model high strains are found out to 20 m.

In order to have better understanding of the stress distribution in the soil when the train is passing and identify the region that behaves nonlinearly, the octahedral shear strain in the *y-z* plane below the first and fourth axle loads is shown in Fig. 12, for load speeds of 19 m/s and 56.7 m/s from the northbound runs. At a load speed of 19 m/s the strains are similar below the two axles, but the maximum strain occurs below the fourth axle location. For the higher load speed, a larger region of high strain occurs at the first axle location and the maximum strain occurs at this position. Based on the shear modulus reduction curve [5], the shear modulus starts to degrade significantly when the strain level exceeds 0.1% for the organic clay.
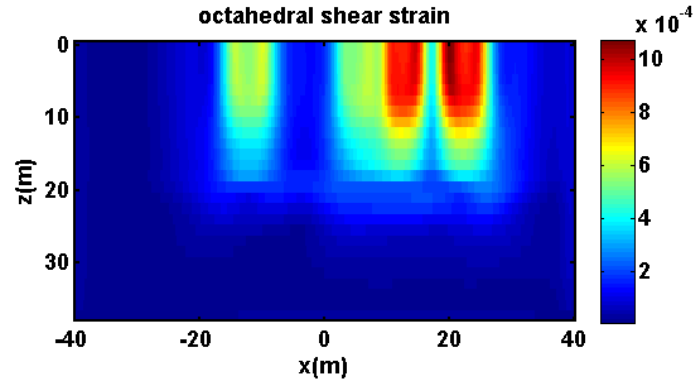
(a)
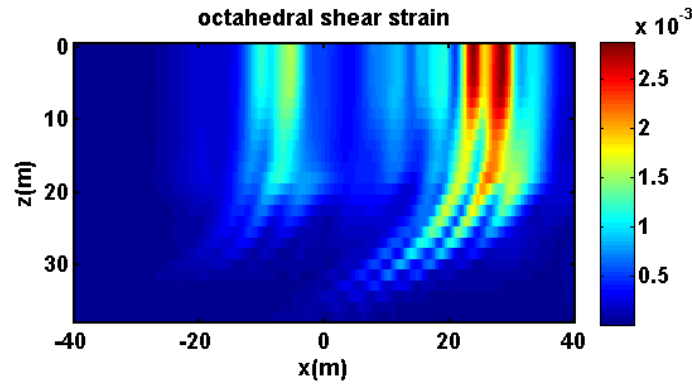
(b)

Figure 11. Octahedral shear strain at the top surface of the organic clay layer from linear and nonlinear model at load speed 56.7m/s (Northbound); (a) linear model; (b) nonlinear Model 2

As can be seen from Fig. 12, the maximum octahedral shear strain occurs in the organic clay layer, between 1.1 m and 4.1 m below the surface, which is the softest layer of the whole system. For the lower speed, only a small region is found with strain levels higher than 0.001, which is at the top of the organic clay layer for the first axle and at the bottom of the organic clay for the 4th axle load. For the higher load speed, the region of high strain under the leading axle becomes deeper. Furthermore, a wider region is found with strain level higher than 0.001 for the 4th axle load
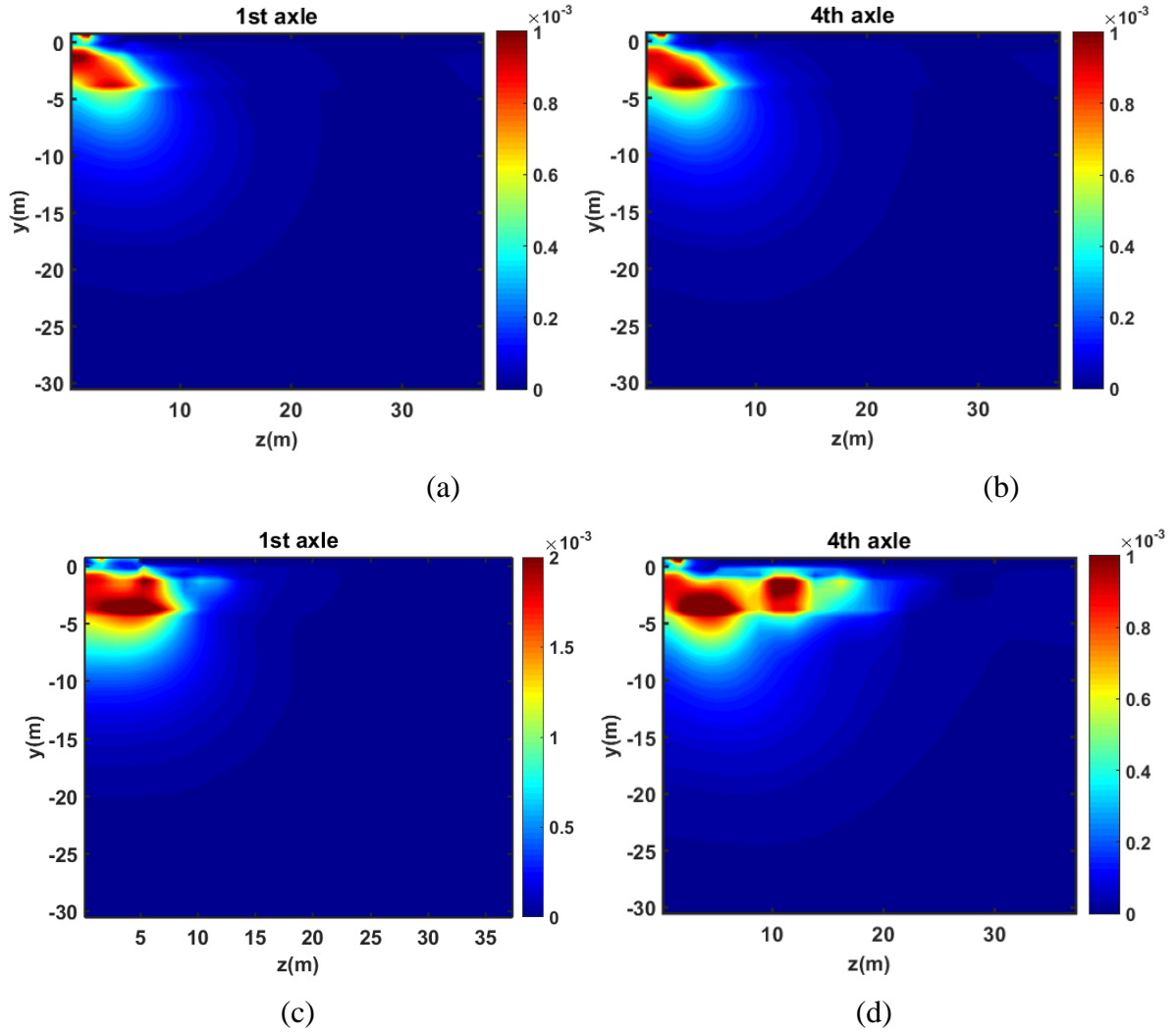
Figure 12. Octahedral shear strain in the *y-z* plane below the first and fourth axles for different load speeds (northbound); (a) V=19 m/s, 1st axle; (b) V=19 m/s, 4th axle; (c) 56.7 m/s, 1st axle; (d) 56.7m/s, 4th axle

4.4 Assessment of critical speed

The maximum upward and downward sleeper displacements obtained for different train speeds are shown in Fig. 13. Results are shown from the site measurements [5], the linear model and the second nonlinear model. The critical speed, identified as the speed at which the maximum deflection occurs, is found at around ~57 m/s. A similar value is also identified in the literature [1], [4], [5], [31]. Good agreement is found between the measurements and the nonlinear model. The maximum downward displacement at the critical speed, at around 15 mm, is roughly double the result obtained due to the static load. On the other hand, the linear model predicts a critical speed of around 70 m/s, which is ~25% higher than the result from the nonlinear model. Furthermore, the maximum deflections close to the critical speed are much smaller for the linear model than for the nonlinear one. It is clear that soil

19

nonlinearity should be considered for this site at the higher train speeds, although the results from the linear model agree reasonably well with the measurements for speeds lower than 40 m/s.
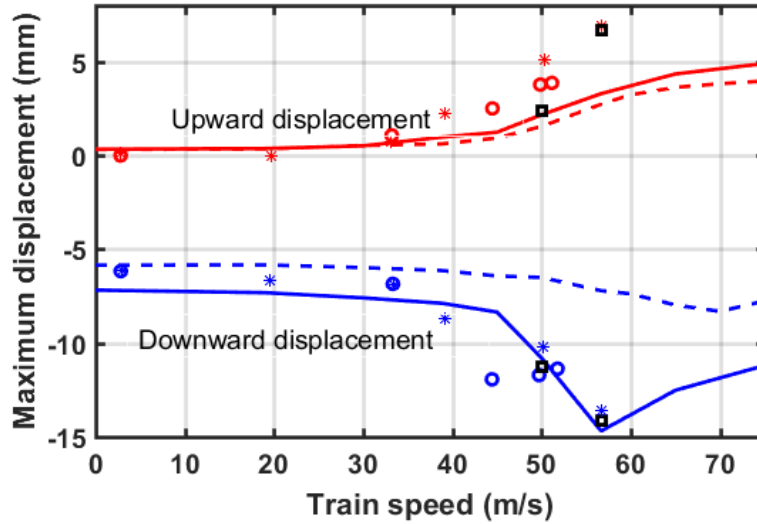

Figure 13. Maximum upward and downward sleeper displacements for different train speeds; -: northbound nonlinear model; □: southbound nonlinear model; --: linear model; o: northbound measurement data; *: southbound measurement data

Fig. 14(a) shows the maximum octahedral shear strains at different depths within the organic clay layer obtained from the nonlinear model for different train speeds. In each case the maximum strain at a given depth is shown. The strain level increases significantly when the load speeds are higher than around 45 m/s and reaches a level at higher speeds that is around three times larger than the results at low speed. Comparing these values with the modulus reduction curves in Fig. 5 it can be seen that the modulus will be reduced to between 90% and 70% of the small strain stiffness (according to nonlinear model 2).

Although the maximum deflections were identified in Fig. 13 as occurring at 57 m/s, the maximum octahedral shear strains occur at higher speeds for depths of 2.75 m and 3.8 m. To investigate the effect of depth further, Fig. 14(b) shows the maximum upward and downward deflections occurring at these depths. The maximum downward deflection occurs at around 57 m/s for each depth. Thus larger octahedral shear strains do not necessarily correspond to larger deflections.
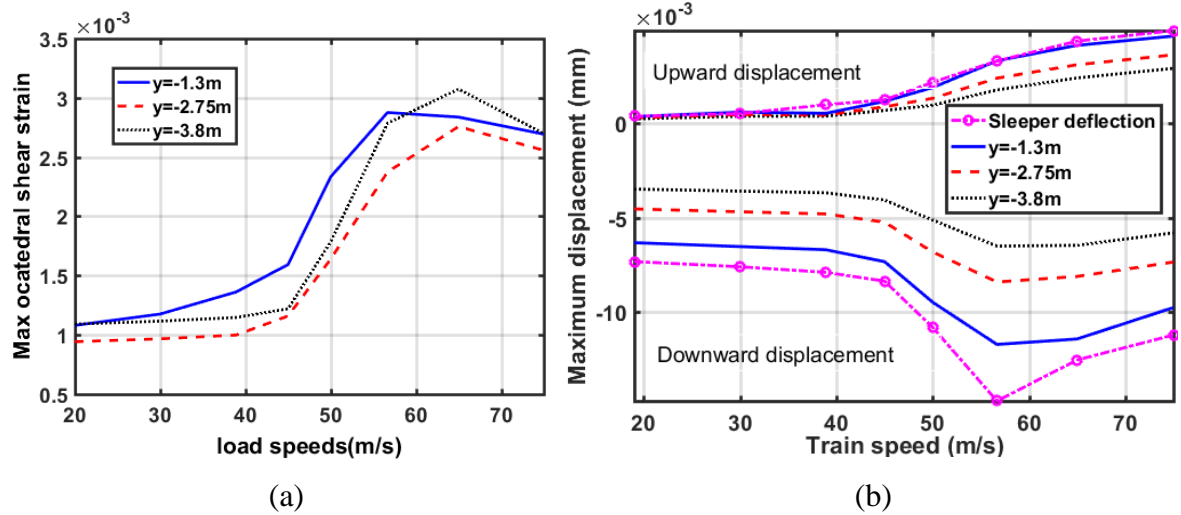
Figure 14. Maximum octahedral shear strain level and deflection at various depths in the organic clay layer at different load speeds from nonlinear model; (a) octahedral shear strain level; (b) maximum upward and downward deflection

4.5 Summary

It is clear from the results presented in this section that incorrect behaviour can be found if the soil nonlinearity is neglected in the model. The linear model underestimates the displacements while it slightly overestimates the critical speed. Furthermore, the strain levels from the linear model are much smaller than those from the nonlinear model when the load speed approaches the critical speed. Nevertheless, the linear model gives acceptable results for lower speeds where the strains are less than about 10^{-3}.

5. Equivalent linear model

5.1 Procedure

Even though better agreement is found by using a nonlinear model, such a model tends to be much more computationally expensive than a linear model, in the present cases by about a factor of 20. Therefore, an equivalent linear model, as used by previous authors [1], [4], [5], [12] is considered here as an alternative. Although time domain simulations are compared here, equivalent linear models can be also implemented in the frequency domain which can give improved efficiency. This is one of the main advantages of the equivalent linear approach.

The equivalent linear model is an approximate approach that can account for soil nonlinearity to some extent. An iterative procedure based on the effective shear strain is required in order to achieve convergence. Convergence can be assumed if the difference between the shear

modulus and damping ratio obtained in successive iterations is less than about 5~10% [16]. An effective shear strain is required to characterise the strain level from a transient record. This is often defined as

$$\gamma_{eff} = R_r \gamma_{max} \tag{7}$$

where R_r is an empirical factor usually between 0.2 and 1 [22], [24] and γ_{max} is the maximum shear strain level for a specific layer [16]. As a result, a medium that is inhomogeneous with depth is obtained. This methodology has been used previously for calculations of the track/ground deflections induced by moving trains [1], [4]. In a variation of this approach, instead of defining the same material modulus for an entire layer, Costa et al. allowed the material to be inhomogeneous in the width direction as well by identifying the maximum shear strain level element by element [5].

An approximate shear modulus reduction is used in references [1], [4], [12] without any iteration. The procedure introduced by Costa et al. [5] requires more iterations to get to convergence because the criterion is applied to each element in the cross-section instead of an entire layer. Here a simpler equivalent linear analysis based on the procedure given in [16] is considered owing to the practical difficulties of updating every element at each iteration in the commercial software. Even though the strain distribution is different in the present case from the 1D wave propagation considered in [16], the interest of the present paper is focussed on the region close to the track where it can be expected that relatively good predictions can be obtained. However, a more thorough procedure such as that given in [5] would be needed to determine the far-field response. Again γ_{oct} is used here instead of the shear strain to determine the maximum strain, due to the complex three-dimensional strains occurring during train passage, as mentioned in Section 2. This was also used in [5], [37].

Curves of the shear modulus reduction and damping ratio for the embankment, crust, organic clay and clay are used, as shown in Fig. 2 [5]. Based on the conclusions from Section 4, the shear modulus reduction curve and damping ratio from the second nonlinear model (Fig. 5) are used for investigating the factor to calculate the appropriate effective shear strain.

5.2 Investigation of the value R_r for the equivalent linear model based on nonlinear results

The influence of using different values of R_r is discussed here. For convenience, to avoid extensive iterations, the maximum strain level from the nonlinear model is used as the initial iteration for the equivalent linear analysis. To determine the next iteration, the maximum octahedral shear strain at each depth is determined from the results of the nonlinear model. These are converted to effective strain by multiplying by the chosen value of R_r according to Eq. (7). From the effective strain, reduced shear modulus values are determined and used in a linear analysis. Further iterations are carried out as necessary. The results from this second iteration are compared with those from the previous step (i.e. the nonlinear model) in Fig. 15 and 16 for values of R_r of 0.65 and 0.2. This shows the shear modulus reduction and damping ratio that are input to the model for the next step. Note that the values of shear modulus plotted at the first step are not those used in the nonlinear model; they are the values of reduced shear modulus obtained from the maximum strains coming from the nonlinear model. They are different in Fig. 15 and 16 due to the use of different factors R_r.

If convergence has been achieved, the difference in shear modulus reduction and damping ratio between successive iterations should be less than 5~10% [16]. From Fig. 15, the results obtained using $R_r = 0.65$ at 56.7 m/s show differences of around 25% between the first and second iteration, whereas the results for $R_r = 0.2$ in Fig. 16 show much smaller differences indicating convergence has been achieved.
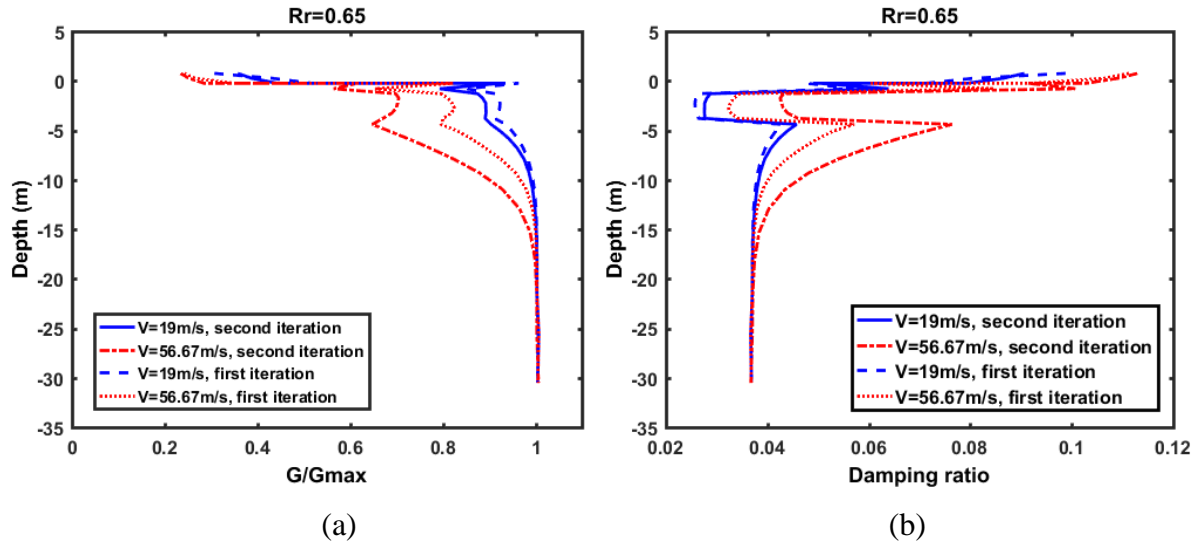
Figure 15. Variation of shear modulus reduction and damping ratio with depth obtained using R_r=0.65 for two different load speeds, showing initial results and results after two iterations; (a) shear modulus reduction; (b) damping ratio
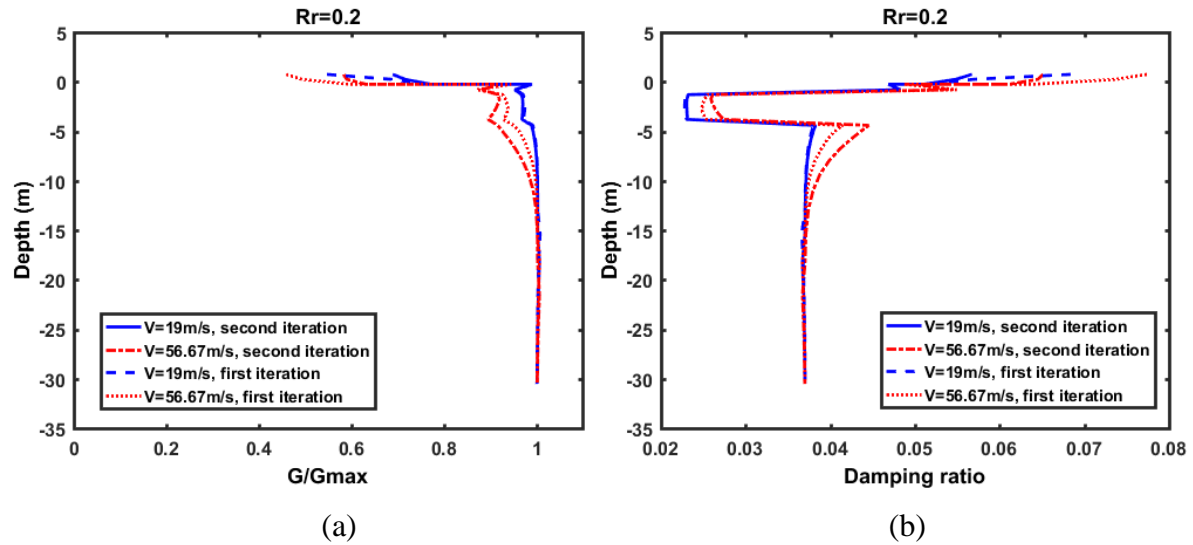

Figure 16. Variation of shear modulus reduction and damping ratio with depth obtained using R_r =0.2 for two different load speeds, showing initial results and results after two iterations; (a) shear modulus reduction; (b) damping ratio

Looking at this a different way, the distributions of shear strain over the transient record can be considered. In order to able to choose an appropriate equivalent value that can capture the correct dynamic behaviour during the nonlinear analysis, the cumulative distribution function is used here. Fig. 17 shows the cumulative distribution functions of the normalized octahedral shear strain level obtained from the nonlinear model at the top surface of the organic clay. Results are shown for four different locations, from 0.7 m to 5.3 m away from the track

centreline. In each case the value is normalized by the maximum strain at that position. From these results it can be seen that the median value (cumulative distribution function of 0.5) occurs at around a normalised strain of 0.2 for the locations close to the track.
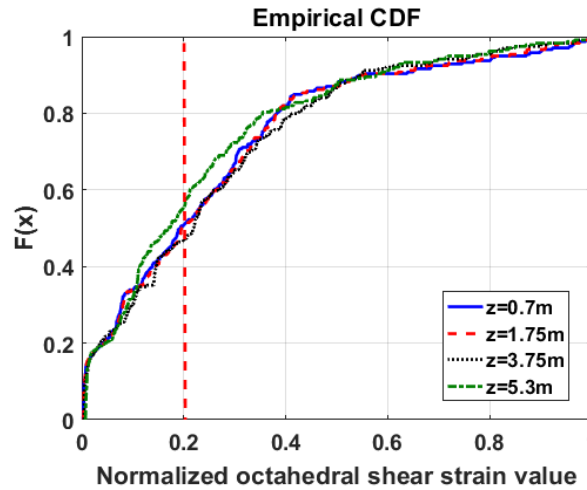

Figure 17. Cumulative distribution function of octahedral shear strain at load speed 56.7 m/s for the top surface of organic clay layer

The maximum octahedral shear strain as a function of the depth for two different train speeds obtained in the converged results from the equivalent linear analysis with different values of R_r are compared with the results from linear and nonlinear models in Fig. 18. As can be seen, the strain levels are typically 10^{-3}, which is too large to allow the use of the small strain approximation (see Fig. 5). Nevertheless, for the load speed of 19 m/s, small differences are found between the four different models, confirming that it is unnecessary to take soil nonlinearity into account in this case, whereas Fig. 18(b) shows that for a load speed of 56.7 m/s the maximum strain level in the organic clay layer is around 57% higher for the nonlinear model than for the linear model. Furthermore, the strain level with R_r=0.2 is very similar to the results from the nonlinear model whereas the strain level is overestimated by around a factor of 2 when 0.65 is used. Finally, Fig. 19 shows the time histories of track displacement for the southbound train. These agree well with the measurements when 0.2 is used for the equivalent linear analysis, whereas they are overestimated when using the factor of 0.65.

Although 0.2 appears to be the most suitable value for R_r in the current case study of track deflections at Ledsgård, further investigation is required in order to reach a more general conclusion that can be applied to other sites and to displacements further from the track.
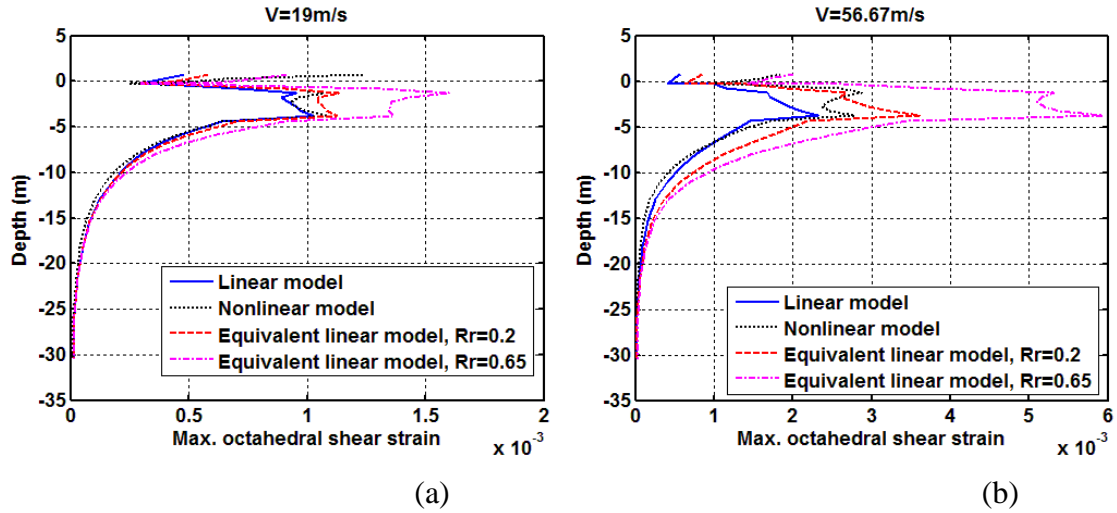
Figure 18. Variation of maximum octahedral shear strain with depth for two different speeds;
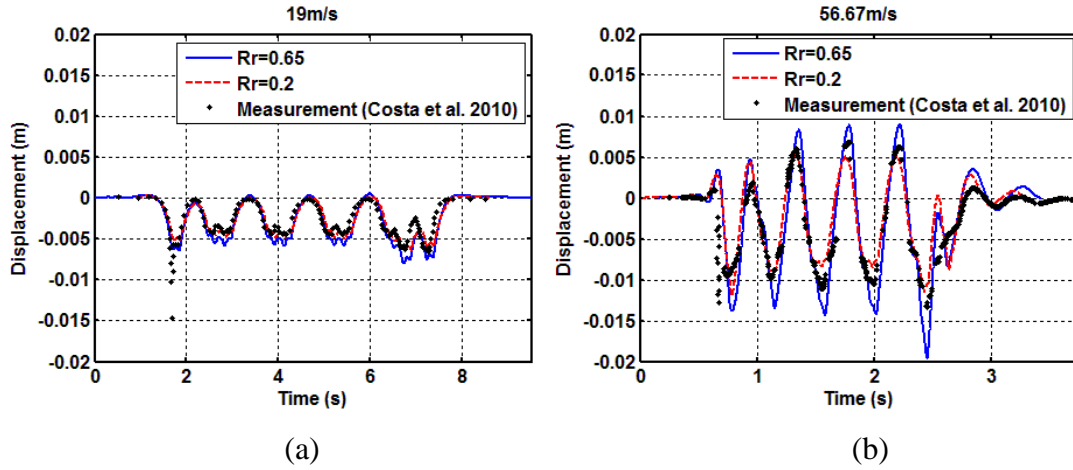(a) V=19 m/s; (b) V=56.7 m/s

Figure 19. Displacement for southbound train from equivalent linear model; (a) V=19 m/s; (b)
V=56.7 m/s

6. Conclusions

A three-dimensional track/ground finite element model that includes soil nonlinearity has been developed that operates in the time domain. Soil nonlinearity has been implemented within the FE model in terms of shear modulus degradation curves based on laboratory results. Good agreement has been found compared with site measurements at the soft soil site in Ledsgård, Sweden. The effect of soil nonlinearity becomes significant at this site when the load speeds approach or exceed the critical speed. The maximum track displacements for load speeds close to the critical speed are around twice those found at lower speeds. The maximum strain levels in the subgrade increase by around a factor of three.

A linear model based on the small strain stiffnesses gives good results for low speeds, up to around 70% of the critical speed. Good agreement is found compared to the results from nonlinear model not only for sleeper displacement but also the maximum octahedral shear strain along the depth. However, the critical speed obtained from this linear model is ~25% higher than that obtained from the nonlinear model and the displacements from the linear model are underestimated for speeds approaching the critical speed.

Two different shear modulus reduction curves have been considered here in the nonlinear model, both of which are broadly consistent with soil data obtained in triaxial tests. The results are found to be very sensitive to the choice of this curve. The damping is based on constant Rayleigh coefficients but it is found that the damping ratio increases due to the stiffness degradation and this fits the data from triaxial test quite well.

The maximum strain levels are found in the organic clay layer, which is the softest layer. High strain levels can be found for the higher load speed at the region under the leading axle. On the other hand, a wider region is found that has strain level larger than 0.001 at the following axle. Octahedral shear strains of around 10^{-3} can still be found at 30 m away from the track for the nonlinear model.

Finally, results from an equivalent linear approach are compared with the results from the nonlinear model. From this it is shown that consistent results are found if the equivalent strain is taken as 20% of the maximum strain value. This shows better agreement with the nonlinear analysis and the measurements than the conventional factor of 65% used in earthquake analysis. Nevertheless, further investigation is required in order to reach a more general conclusion that can be applied to other sites and to displacements further from the track.

Appendix A. Shear modulus reduction curve

The shear modulus reduction curve is based on the following functions proposed by Ishibashi et al. [18] in terms of cyclic shear strain amplitude, mean effective confining pressure and the soil's plasticity index. The shear modulus reduction is written as

$$\frac{G}{G_{max}} = K\left(\gamma, I_p\right)\bar{\sigma}_0^{\,m\left(\gamma, I_p\right)-m_0} \tag{A1}$$

where $\bar{\sigma}_0$, γ, I_p are the mean effective confining pressure, cyclic shear strain amplitude and plasticity index. When the shear strain is smaller than 10^{-6}

$$K\left(\gamma, I_p\right) = 1 \tag{A2}$$

$$m\left(\gamma, I_p\right) - m_0 = 0 \tag{A3}$$

For shear strains larger than 10^{-6}

$$K\left(\gamma, I_p\right) = 0.5\left\{1 + \tanh\left[\ln\left(\frac{0.000102 + n\left(I_p\right)}{\gamma}\right)^{0.492}\right]\right\} \tag{A4}$$

$$m\left(\gamma, I_p\right) - m_0 = 0.272\left\{1 - \tanh\left[\ln\left(\frac{0.000556}{\gamma}\right)^{0.4}\right]\right\}e^{-0.0145 I_p^{1.3}} \tag{A5}$$

where

$$n\left(I_p\right) = \begin{cases} 0.0 & \text{for} & I_p = 0 \\ 3.37\times10^{-6} I_p^{1.404} & \text{for} & 0 \leq I_p \leq 15 \\ 7.0\times10^{-7} I_p^{1.976} & \text{for} & 15 \leq I_p \leq 70 \\ 2.7\times10^{-5} I_p^{1.115} & \text{for} & I_p > 70 \end{cases} \tag{A6}$$

References

[1]   C. Madshus and A. M. Kaynia, "High-speed railway lines on soft ground: dynamic behaviour at critical train speed," *J. Sound Vib.*, vol. 231, no. 3, pp. 689–701, 2000.

[2]   X. Sheng, C. J. C. Jones, and M. Petyt, "Ground vibration generated by harmonic load acting on a railway track," *J. Sound Vib.*, vol. 225, no. 1, pp. 3–28, 1999.

[3]   V. V Krylov, "Generation of ground vibrations by superfast trains," *Appl. Acoust.*, vol. 44, no. 2, pp. 149–164, 1995.

[4]   A. M. Kaynia, C. Madshus, and P. Zackrisson, "Ground vibration from high-speed trains: prediction and countermeasure," *J. Geotech. Geoenvironmental Eng.*, vol. 126, no. 6, pp. 531–537, Jun. 2000.

[5]   P. A. Costa, R. Calçada, A. S. Cardoso, and A. Bodare, "Influence of soil non-linearity on the dynamic response of high-speed railway tracks," *Soil Dyn. Earthq. Eng.*, vol. 30, no. 4, pp. 221–235, Apr. 2010.

[6]   X. Sheng, C. J. C. Jones, and D. J. Thompson, "Modelling ground vibration from railways using wavenumber finite- and boundary-element methods," *Proc. R. Soc. A Math. Phys. Eng. Sci.*, vol. 461, no. 2059, pp. 2043–2070, Jul. 2005.

[7]   Y. B. Yang, H. H. Hung, and D. W. Chang, "Train-induced wave propagation in layered soils using finite/infinite element simulation," *Soil Dyn. Earthq. Eng.*, vol. 23, no. 4, pp. 263–278, 2003.

[8]   S. H. Ju, J. R. Liao, and Y. L. Ye, "Behavior of ground vibrations induced by trains moving on embankments with rail roughness," *Soil Dyn. Earthq. Eng.*, vol. 30, no. 11, pp. 1237–1249, Nov. 2010.

[9]   P. A. Costa, R. Calçada, and A. S. Cardoso, "Track–ground vibrations induced by railway traffic: In-situ measurements and validation of a 2.5D FEM-BEM model," *Soil Dyn. Earthq. Eng.*, vol. 32, no. 1, pp. 111–128, 2012.

[10]   G. Lombaert and G. Degrande, "Ground-borne vibration due to static and dynamic axle loads of InterCity and high-speed trains," *J. Sound Vib.*, vol. 319, no. 3–5, pp. 1036–1066, 2009.

[11]   X. Sheng, C. J. C. Jones, and D. J. Thompson, "A comparison of a theoretical model for quasi-statically and dynamically induced environmental vibration from trains with measurements," *J. Sound Vib.*, vol. 267, no. 3, pp. 621–635, 2003.

[12]   L. Hall, "Simulations and analyses of train-induced ground vibrations in finite element models," *Soil Dyn. Earthq. Eng.*, vol. 23, no. 5, pp. 403–413, Jul. 2003.

[13]   A. El Kacimi, P. K. Woodward, O. Laghrouche, and G. Medero, "Time domain 3D finite element modelling of train-induced vibration at high speed," *Comput. Struct.*, vol. 118, pp. 66–73, Mar. 2013.

[14]   G. Kouroussis, O. Verlinden, and C. Conti, "Ground propagation of vibrations from railway vehicles using a finite/infinite-element model of the soil," *Proc. Inst. Mech. Eng. Part F J. Rail Rapid Transit*, vol. 223, no. 4, pp. 405–413, 2009.

[15]   J.-Y. Shih, D. Thompson, and A. Zervos, "Assessment of track-ground coupled vibration induced by high-speed trains," in *The 21st International Congress on Sound and Vibration*, 2014, no. July, pp. 13–17.

[16]   S. L. Kramer, *Geotechnical Earthquake Engineering*. Prentice-Hall, Inc., 1996.

[17]   I. A. Beresnev and K. Wen, "Nonlinear Soil Response A Reality ?," *Bull. Seismol. Soc. Am.*, vol. 86, no. 6, pp. 1964–1978, 1996.

[18]   I. Ishibashi and X. Zhang, "Unified dynamic shear moduli and damping ratio of sand and clay," *Soils Found.*, vol. 33, no. 1, pp. 182–191, 1993.

[19]   T. Iwasaki, F. Tatsuoka, and Y. Takagi, "Shear moduli of sand under cyclic torsional shear loading," *Soils Found.*, vol. 18, no. 1, pp. 39–56, 1978.

[20]   T. Kokusho, "Cyclic triaxial test of dynamic soil properties for wide strain range," *Soils Found.*, vol. 20, no. 2, pp. 45–60, 1980.

[21]   P.-N. Thach, H.-L. Liu, and G.-Q. Kong, "Vibration analysis of pile-supported embankments under high-speed train passage," *Soil Dyn. Earthq. Eng.*, vol. 55, pp. 92–99, Dec. 2013.

[22]   N. Yoshida, S. Kobayashi, I. Suetomi, and K. Miura, "Equivalent linear method considering frequency dependent characteristics of stiffness and damping," *Soil Dyn. Earthq. Eng.*, vol. 22, pp. 205–222, 2002.

[23]   K. Miura, S. Kobayashi, and N. Yoshida, "Equivalent linear analysis considering large strain and frequency dependent charactersitics," in *12th World Conf. on Earthq. Eng*, 2000, pp. 1832–1839.

[24]   I. Katayama, K. Ozeki, A. Yamaya, and Y. Seshimo, "Non-linear free-field soil response analysis of a vertical array data," *Tech. Rep. NCEER*, pp. 735–761, 1992.

[25]   J. Sadeghi, "Investigation of characteristics and modelling of railway track system," PhD thesis at University of Wollongong, 1997.

[26]   W. D. Iwan, "On a class of models for the yielding behavior of continuous and composite systems," *J. Appl. Mech.*, vol. 34, no. 3, pp. 612–617, 1967.

[27]   A. Gomes Correia and J. Cunha, "Analysis of nonlinear soil modelling in the subgrade and rail track responses under HST," *Transp. Geotech.*, vol. 1, no. 4, pp. 147–156, Dec. 2014.

[28]   V. A. Fernandes, "Numerical analyis of nonlinear soil behavior and heterogeneity effects on railway track response," PhD thesis at École Centrale Paris, 2014.

[29]   A. Kalliainen, P. Kolisoja, and A. Nurmikolu, "3D Finite Element Model as a Tool for Analyzing the Structural Behavior of a Railway Track," *Int. Conf. Transp. Geotech. (ICTG 2016)*, vol. 143, pp. 820–827, 2016.

[30]   B. Indraratna, W. Salim, and C. Rujikiatkamjorn, *Advanced Rail Geotechnology – Ballasted track*. CRC Press, 2011, p. 414.

[31] P. K. Woodward;, O. . Laghrouche, S. B. . Mezher, and D. P. Connolly, "Application of coupled train-track modelling of critical speeds for high-speed trains using three-dimensional non-linear finite elements," *Int. J. Railw. Technol.*, vol. 4, no. 3, pp. 1–35, 2015.

[32] J.-Y. Shih, D. J. Thompson, and A. Zervos, "The effect of boundary conditions, model size and damping models in the finite element modeling of moving load on a track/ground system," *Soil Dyn. Earthq. Eng.*, vol. 89, pp. 12–27, 2016.

[33] J.-Y. Shih, D. J. Thompson, and A. Zervos, "Modelling scheme for railway vehicle/track/ground dynamic interaction in the time domain," in *The 24th International Conference on Computational Mechanics (ACME-2016).*

[34] X. Sheng and C. J. C. Jones, "Ground vibration generated by a load moving along a railway track," *J. Sound Vib.*, vol. 228, no. 1, pp. 129–156, 1999.

[35] H. A. Dieterman and V. A. Metrikine, "Steady state displacements of a beam on an elastic half space due to a uniformly moving load," *Eur. J. Mech. - A/Solids*, vol. 16, no. 2, pp. 295–306, 1997.

[36] M. Lieb and B. Sudret, "A fast algorithm for soil dynamics calculations by wavelet decomposition," *Arch. Appl. Mech.*, vol. 68, no. 3, pp. 147–157, 1998.

[37] A. M. Halabian and M. H. El Naggar, "Effect of non-linear soil – structure interaction on seismic response of tall slender structures," *Soil Dyn. Earthq. Eng.*, vol. 22, pp. 639–658, 2002.